ACS OMEGA

http://pubs.acs.org/journal/acsodf

Article

Synthesis of Carbon Dots with Hemostatic Effects Using Traditional Chinese Medicine as a Biomass Carbon Source

Bingchen Han, Lidan Shen, Hanbing Xie, Qi Huang, Dan Zhao, Xianju Huang, Xiao Chen, and Jun Li*

Cite This: *ACS Omega* 2023, 8, 3176−3183

Read Online

ACCESS | Metrics & More | Article Recommendations | Supporting Information

ABSTRACT: As novel nanomaterials developed gradually with nanotechnology, carbon dots have been widely applied in medical applications, including disease treatment, drug delivery, antibacterial applications, and phototherapy. Based on the similar process between Chinese medicinal materials for hemostasis and modern carbon dots, this paper reports the preparation of four luminescent carbon dots with Chinese medicinal materials (plants and animals) as carbon sources and the investigation on their hemostatic effects in vitro and in rat bleeding models. It is found that the four studied carbon dots exhibit similar hemostatic effects and hemostatic mechanisms through impacting both endogenous and exogenous coagulation pathways. In addition, these carbon dots all exhibit anti-inflammatory effects and good biocompatibility, ensuring their potential in pretraumatic fields. This work provides a new perspective for hemostatic carbon dots prepared using carbonized natural plants and animals and new ideas for the research of new hemostatic materials.

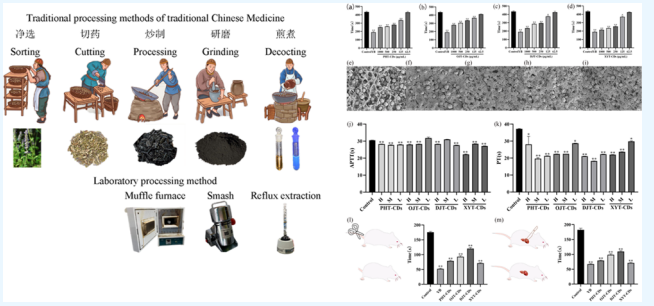

1. INTRODUCTION

As an important type of fluorescent carbon-based nanomaterials, carbon dots (CDs) have exhibited better chemical stability and relatively long systemic circulation in the human body and thus have promising potentials in biochemical applications. Due to their small particle sizes (smaller than 10 nm), carbon dots possess excellent water dispersibility and easy functionalization for further enhanced optical properties.[1,2] Compared with semiconductor quantum dots, CDs have higher photobleaching resistance, better biocompatibility, and lower toxicity,[3] and their emission wavelengths depend on the particle size, crystallinity, and surface chemical properties. CDs could produce reliable optical signals and can be rapidly removed from the body.

The appearance of carbon dots has provided new possibilities and methods for the detections and treatments of various diseases, such as antibacterial,[4−6] anticancer,[7,8] chemotherapy,[9,10] photothermal therapy,[11,12] and photodynamic therapy.[13]

For thousands of years, Chinese people have been using various medicinal materials to make charcoal medicine for hemostasis, which has been recorded as being used for trauma-caused bleedings and diseases of people and animals in ancient Chinese medical books. The earliest record was in the ancient medical book Prescriptions for Fifty-Two Diseases in the third century B.C., and so far, there have been many charcoal medicines for hemostasis recorded in the Chinese Pharmacopoeia.

The carbon medicines are prepared through carbonization of medicinal materials at high temperature, similar to the top-to-bottom formation mechanism of carbon dots, and have been reported to contain carbon dots and to be effective in disease treatment.[14−16] For instance, the carbon dots synthesized from Coptis chinensis have protective effects on acute kidney injury induced by Agkistrodon acutus venom.[17] Zhang et al. discovered that the carbon dots prepared with jujube as the carbon source can promote the growth of red blood cells and can be used as a potential drug to treat anemia,[18] providing a new perspective for developing hemostatic drugs.

Three charcoal medicines have been prepared with a muffle furnace to simulate the processing of traditional Chinese medicine, with the dried pollen of *Typha angustifolia* L., dry rhizome node of *Nelumbo nucifera* Gaerth., and dry rhizome node of *Cirsium japonicum Fisch. ex DC.* as carbon sources. The fourth charcoal medicine (made from adult healthy human hair) was purchased from the market (the medicine was first dispersed in ultrapure water and then processed through ultrafiltration and centrifugation and purification through a dialysis belt.). The optical and physicochemical properties of these four carbon dots and their biocompatibility have been studied, and their activities in the pretraumatic stage, including hemostasis and anti-inflammation, have been investigated. It

Received: October 13, 2022
Accepted: December 26, 2022
Published: January 10, 2023

was discovered that these four carbon dots exhibited different antitrauma effects, providing a reference for new hemostatic materials and the development of new hemostatic drugs.

1.1. Preparation and Characterization of CDs. The method of preparation was slightly improved from the operation in the references. A total of 500 g of the dried pollen of *T. angustifolia* L. was put in a crucible, which was then wrapped with tin foil and put in a muffle furnace and heated at 300 °C for 1 h. It was then removed and sprinkled with water to remove sparks; after that, it was dried in a ventilated place.

Next, 500 g of dry rhizome node of *N. nucifera* Gaerth. was taken and operated as the dried pollen of *T. angustifolia* L., except that it was heated at 450 °C in a muffle furnace for 1 h. A total of 500 g of dry rhizome node of *Cirsium japonicum Fisch. ex DC.* was taken and operated in the same way, except being heated at 350 °C for 1 h in a muffle furnace.

A total of 100 g of the three carbonized medicinal materials and 100 g of the residual blood carbon were taken, and after the pulverization, 500 mL of water was used to reflux and extract at 100 °C for 1 h. The solution was then cooled, preliminarily filtered, and further filtered through a 0.22 μm microporous filter membrane. The obtained solution was placed in a 3000 Da dialysis bag for dialysis for 7 days, and the water was changed every 12 h. The solution in the dialysis belt was taken out and lyophilized to obtain four kinds of carbon dots, which were named as PHT-CDs, OJT-CDs, DJT-CDs, and XYT-CDs (prepared from the dried pollen of *T. angustifolia* L., dry rhizome node of *N. nucifera* Gaerth., dry rhizome node of *Cirsium japonicum Fisch. ex DC.*, and healthy human hair).

A series of instruments have been used to characterize the prepared carbon dots to obtain their optical characteristics and surface functional groups. The transmission electron spectrum was acquired with a jem-2100plus microscope produced by Japan Electron Optics Laboratory Company, and the ultraviolet−visible spectrophotometer (UV) was a Lambda-35 model from PerkinElmer company, the fluorescence spectrophotometer (FL) was an LS55 model from PerkinElmer company, ζ-potential was taken using a Zen3690 ζ-potential analyzer from Malvern company, Fourier transform infrared spectroscopy (FTIR) was performed using a FTIR spectrophotometer from Thermo Fisher Scientific, X-ray photoelectron spectroscopy (XPS) was taken using a 250xi XPS spectrophotometer from Thermo Fisher Scientific, and the nuclear magnetic resonance spectrometer was an Avance Neo 500m model from Bruker company.

1.2. Cytotoxicity. The cytotoxicities of PHT-CDs, OJT-CDs, DJT-CDs, and XYT-CDs was measured by the CCK-8 method. Raw265.7 cells in the logarithmic growth phase were scraped off with a cell scraper, added with complete medium, and evenly spread in 96-well plates. After the cells were fully cultivated, the cell supernatant was discarded. The blank control group was given blood-free medium, and for the drug group, 500, 400, 300, 200, and 100 μg/mL CDs were added. After 24 h of treatment, a CCK-8 kit was used for detection, and the absorbance values at OD 450 nm were measured using a microplate reader.

1.3. *In Vitro* Compatibility Experiment. A total of 10 mL of phosphate-buffered saline (PBS) was added to 5 mL of rabbit blood, mixed with slight vortex, and centrifuged at 3000*g* for 5 min, and the supernatant was discarded. Next, 10 mL of PBS was added to the lower precipitated red blood cells, and the above-mentioned operations were repeated until the supernatant was basically clear and colorless after centrifugation. The lower precipitated red blood cells were recovered, and the red blood cell concentration was diluted to about 10% with PBS. A total of 0.2 mL of 10% red blood cells was mixed with 0.8 mL of the above-mentioned concentration gradient, and the final concentrations were 125, 250, 500, 1000, 2000, 5000, and 10,000 μg/mL after slight vortex, and 0.2 mL of 10% red blood cells mixed with 0.8 mL of D-PBS was negative, and 0.2 mL of 10% red blood cells mixed with 0.8 mL of distilled water was positive. All groups were incubated at 37 °C for 4 h, and after incubation, they were swirled slightly and centrifuged at 3000*g* centrifugal force for 5 min. A total of 100 μL of supernatant was carefully transferred into 96-well plates, and the absorbances of each group were measured at 577 nm. The hemolysis rate was calculated according to the following formula.

1.4. Anti-inflammatory Effect of CDs on the Inflammation Model of LPS-Induced RAW264.7 Cells. Some changes were made to the operation compared to the method reported in the literature.[19] The RAW264.7 cells in the logarithmic growth period were blown evenly (complete culture medium), and the cell suspension was prepared and evenly spread on 96-well plates. After the cells were fully cultivated, the supernatant was discarded and the blank control group was given serum-free culture medium. The positive control groups were 5 μM dexamethasone and 0.5 μg/mL LPS. The drug groups were 100, 200, 300, 400, and 500 μg/mL of each drug and 0.5 μg/mL LPS. After 12 h of administration, the drug was detected using a NO detection kit, and the absorbances at OD 450 were measured using a microplate reader.

1.5. Coagulation Time of Blood (CBT) of CDs In Vitro. The blood coagulation tests were carried out according to the method described by Wang et al.[20] The sample was added into a 2 mL EP tube, and then, 100 μL of 0.9 mL of rabbit whole blood (3.8% sodium citrate/blood = 1:9) was added. The final concentration of the drug content was then set at 62.5, 125, 250, 500, and 1000 μg/mL. A total of 0.1 mL of 3 mg/mL calcium chloride was added into the EP tube, and the solution was then taken out of the tube at 37 °C (constant-temperature water bath pot) every 10 s and was tilted to see if the blood is coagulated or flows. When the blood was completely coagulated, that is, the inclined centrifuge tube reached 90 and there was no blood flow, the in vitro coagulation time of each group was recorded. Yunnan Baiyao YB 1000 μg/mL was used as the positive control drug, and the operation was repeated three times (add 10 mg/mL calcium chloride if there is no coagulation).

1.6. Determination of Prothrombin Time (PT) and Activated Partial Prothrombin Time (APTT). The determinations of PT and APTT were carried out by referring to the method described by Liu et al.[21] Rabbit whole blood to prepare plasma (within 60 min) was taken, and the specimen was centrifuged at 3000 rpm for 10−15 min, and then, the plasma was stratified. The sample was mixed with plasma evenly so that the final concentration of the drug is 1000, 500, and 100 μg/mL, and the solution was incubated at 37 °C for 3 min and then immediately measured using the relevant kit on an automatic coagulation analyzer (RAC-1830, Shenzhen Leidu Life Science and Technology Co., Ltd.).

1.7. Ultrastructural Observation of Red Blood Cells. The experiments were carried out according to the method

https://doi.org/10.1021/acsomega.2c06600
ACS Omega 2023, 8, 3176−3183

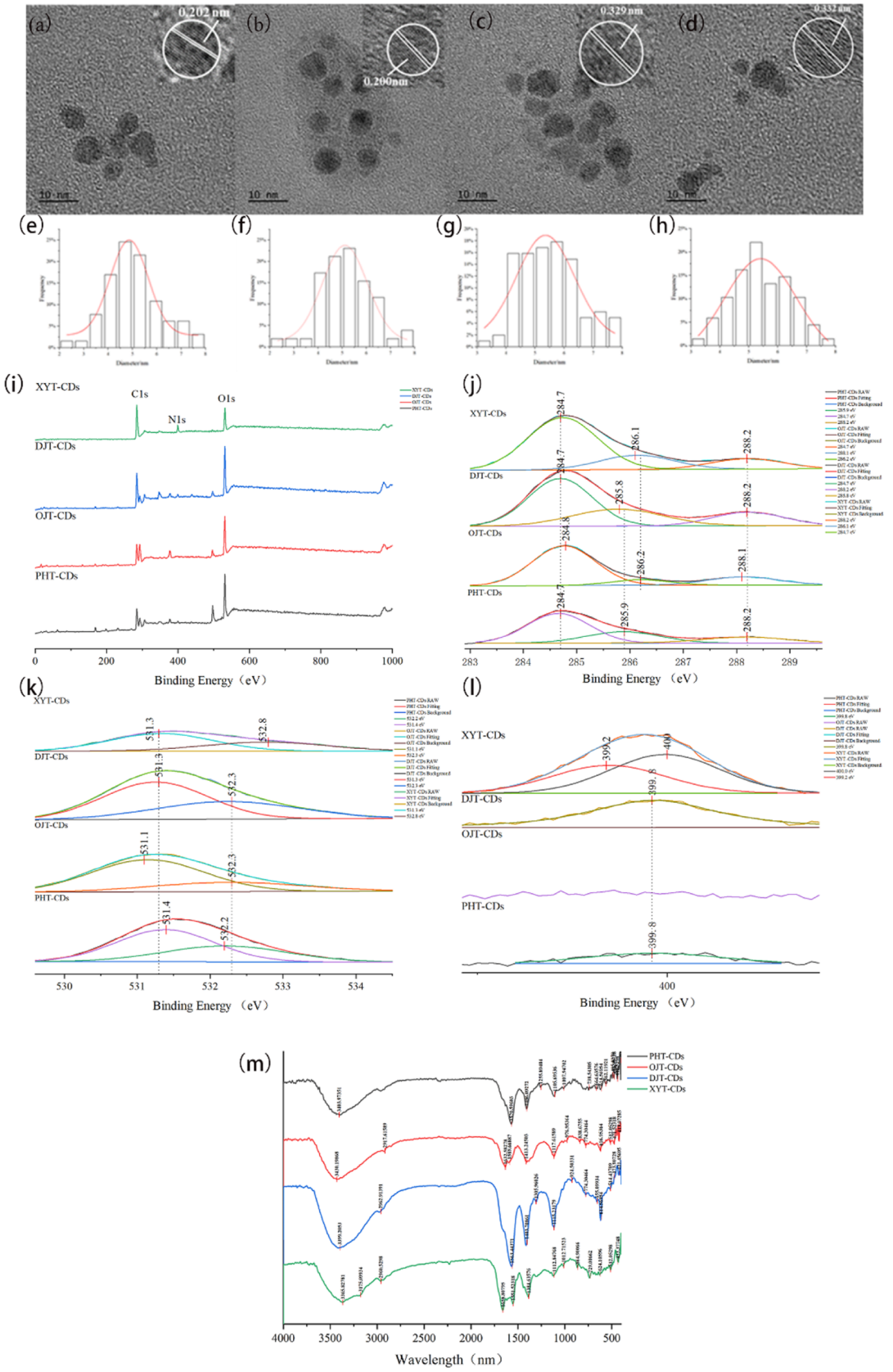

Figure 1. Characterization data of CDs. (a−d) Transmission electron microscopy images of PHT-CDs, OJT-CDs, DJT-CDs, and XYT-CDs, respectively. The illustrations indicate the crystal lattice. (e−h) Particle size distribution histograms of PHT-CDs, OJT-CDs, DJT-CDs, and XYT-CDs, respectively. (i) XPS survey chart, (j) XPS-C 1s, (k) XPS-O 1s, and (l, m) XPS-N 1s.

https://doi.org/10.1021/acsomega.2c06600
ACS Omega 2023, 8, 3176−3183

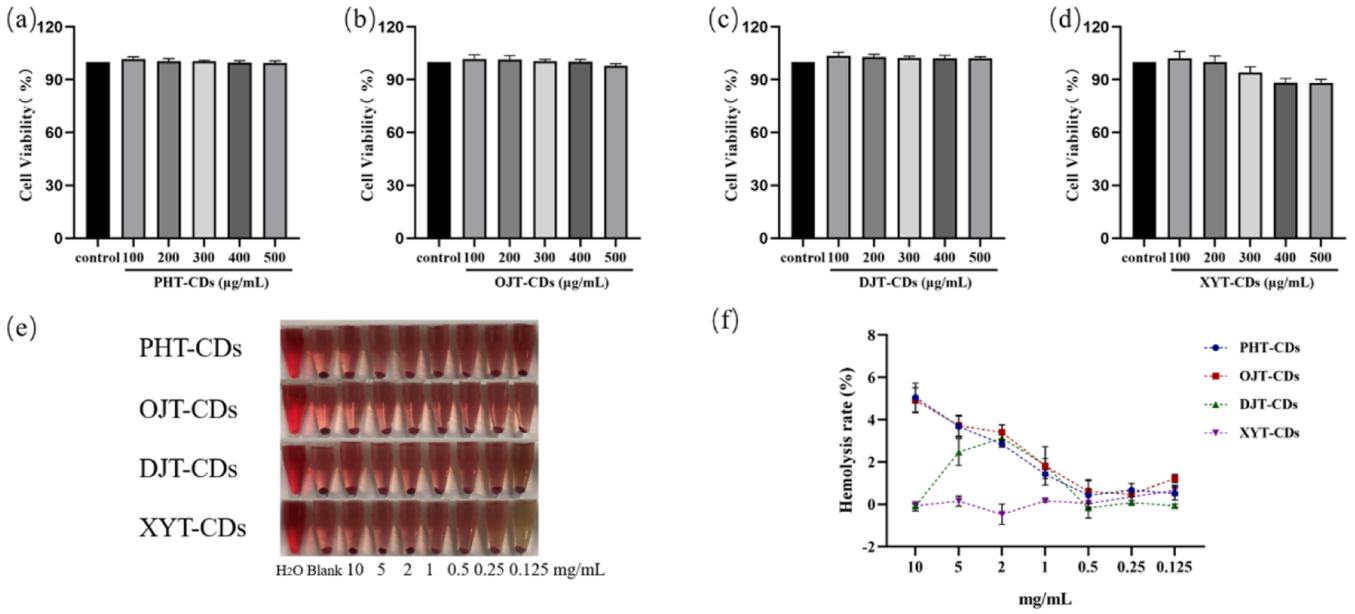

Figure 2. (a–d) Histograms of the cytotoxicity experiment of PHT-CDs, OJT-CDs, DJT-CDs, and XYT-CDs, respectively. (e) Direct view of their hemolysis experiment in vitro. (f) Line graph of their hemolysis rates in vitro.

described by Chen et al.[22] A total of 1 mL of anticoagulated whole blood from rabbit whole blood and the sample (500 μg/mL) were added into the EP tube, and after coagulation, the blood was washed with PBS three times to remove excess red blood cells. 2.5% glutaraldehyde was added, and the solution was fixed at 4 °C for 2.5 h. The clots are dehydrated using gradient ethanol in turn. After drying in vacuum, the aggregation of red blood cells was observed under a scanning electron microscope (SEM, Utral 55,Carl Zeiss).

1.8. Hemostatic Model of Tail Cutting and Liver Laceration in Rats.[23] To prove the hemostatic effect of CDs on body surface wounds, male Sprague–Dawley (SD) rats (90 ± 5 g) were anesthetized by intraperitoneal injection of pentobarbital sodium. Next, 80% of the tail was removed using surgical scissors, and the wound (100 mg) was immediately covered with hemostatic samples. The untreated group was treated with a sterile gauze to suck blood. The bleeding time of each group was recorded. The operation was repeated six times for each sample.

Hair from the liver of SD rats (90 ± 5 g) was removed, and the surgical area was disinfected with 75% alcohol. The liver was cut into 0.5 cm with a 5 mL syringe, and the wound was immediately covered with a 50 mg sample. The blood of the untreated group was absorbed with a sterile gauze. The operation was repeated six times for each sample.

1.9. Statistical Analysis. Data were presented as mean ± standard deviation (SD) and statistically analyzed by one-way analysis of variance with GraphPad.Prism.v.5.0. Measurements were performed in at least triplicate if not stated. The p value < 0.05 was statistically significant.

2. RESULTS AND DISCUSSION

2.1. Characterization of CDs. The fluorescence spectra and ultraviolet spectra of the prepared CDs (PHT-CDs, OJT-CDs, DJT-CDs, and XYT-CDs) are shown in Figures S1–S8, and the four CDs all emit bright blue fluorescence. The ζ-potentials of CDs show that all the carbon dots are negatively charged. The high-resolution transmission electron microscopy (HR-TEM) images (Figure 1a–d) confirmed the formation of quasi-spherical particles with an average particle size of 5.06–5.51 nm. The insets in the images show that PHT-CDs and OJT-CDs possess crystal structures with a lattice spacing of 0.202 and 0.200 nm, attributed to the (102) diffraction plane of graphite (sp).[24] The lattice edge spacing of DJT-CDs is about 0.332 nm and that of XYT-CDs is about 0.339 nm, which are in accordance with the lattice edge spacing of the (002) plane in graphite,[25] indicating that the crystalline core of the prepared CDs has a graphite-like structure (Figure 1e–h). The four carbon dots are in normal distribution and have similar particle size. The XPS spectrum (Figure 1i) shows that most of the elements on the surface of the four CDs are C, O, and N, among which C and O account for about 90%. The content of N in XYT-CDs is higher than that in other carbon dots because the carbon source of XYT-CDs is human hair, which is rich in protein and amino acids. As shown in the C 1s high-resolution XPS spectrum (Figure 1j), all four carbon dots could be fitted into three types of peaks, corresponding to peaks at 284.7, 285.9, and 286.1 and 288.2eV. The high-resolution XPS spectra of O 1s and N 1s shown in (Figure 1k) illustrate that except XYT-CDs, O 1s of other three carbon dots can be fitted as two peaks of 531.3 and 532.3 eV, with less N 1s content. The content of the N element in OJT-CDs is lower than 1%, which can be fitted as one peak, corresponding to 399.8 eV. O 1s of XYT-CDs can be fitted as two peaks, 531.3 and 532.8 eV, and N 1s can be fitted as two peaks, 399.2 and 400 eV. According to the infrared spectrum (Figure 1m), the strong absorption peak at 3369 cm^{-1} is attributed to the existence of O–H and N–H bonds. The weak absorption peak at 2956 cm^{-1} is attributed to the stretching movement of C–H, and the absorption peak at 2238–2387 cm^{-1} is attributed to C–N bonds. The peak at 1301–1562 cm^{-1} proves the existence of C–N and N–H bonds, and the peak at 1118 cm^{-1} shows the existence of C–O bonds. Corresponding to XPS spectra, these results are similar to those of the carbon dots prepared with plants as carbon sources, showing that these carbon dots might have the same structure. However, the

https://doi.org/10.1021/acsomega.2c06600
ACS Omega 2023, 8, 3176–3183

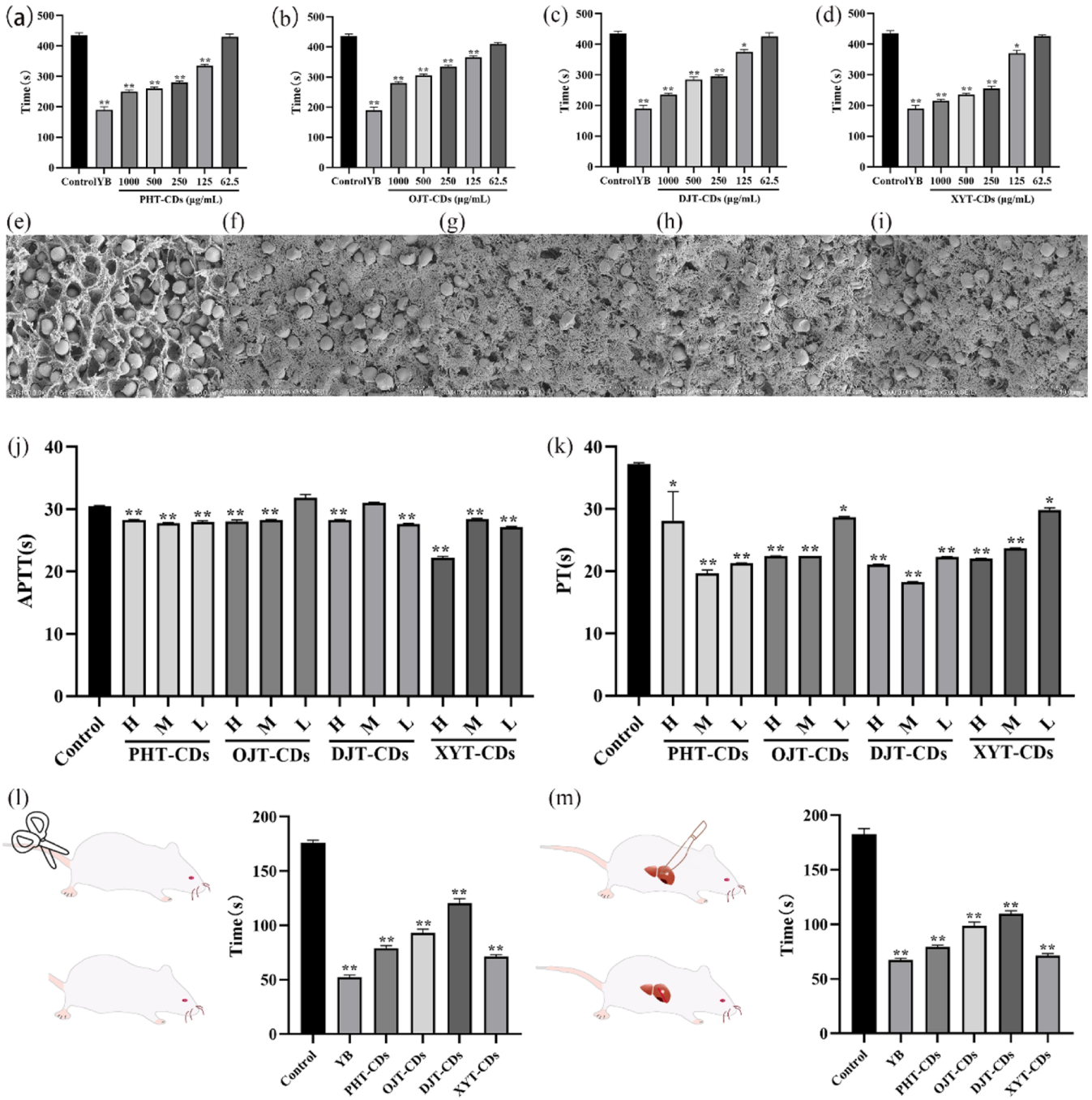

Figure 3. (a−d) Histogram of PHT-CD, OJT-CD, DJT-CD, and XYT-CD in vitro hemostasis experiments, respectively, (e) SEM of the blood clot in the blank control, (f)−(i) SEM of the blood clot after PHT-CD, OJT-CD, DJT-CD, and XYT-CD administration, respectively. (j) APTT histogram. (k) PT histogram. (l) Histogram of bleeding time in the rat tail cutting experiment. (m) Histogram of bleeding time in the rat liver laceration experiment. Compared with the control group, $^{**}P < 0.01$, $^{*}P < 0.05$.

small-molecular compounds rich in traditional Chinese medicine may also participate in the process of carbon dot synthesis, forming rich surface functional groups and providing many possibilities for their applications in medical fields.

2.2. Biocompatibility Evaluation. To evaluate the biocompatibility of the prepared carbon dots, RAW264.7 cells were used to test the cytotoxicity of these four carbon dots. As shown in Figure 2a−d, there was no significant difference between the results of cells treated with different concentrations of carbon dots and the blank control groups, indicating no obvious cytotoxicity from the CDs. In an in vitro hemolysis experiment (Figure 2e), the erythrocyte membrane in the blank control group was destroyed, and hemoglobin flowed out of the erythrocytes. The solution was clear and red, and there was no erythrocyte residue at the bottom of the tubes. In the samples treated with carbon dots, the erythrocytes all sunk to the bottom, and the upper liquid was colorless and clear with the hemolysis rates of the four carbon dots all lower than 5% (Figure 2f). Cytotoxicity and in vitro hemolysis tests proved the excellent biocompatibility of the four carbon dots, which meets the hemolysis rate

https://doi.org/10.1021/acsomega.2c06600
ACS Omega 2023, 8, 3176−3183

requirements for hemostatic materials, and proved their potential in biological applications.

2.3. Hemostatic Effect and Mechanism of Carbon Dots. The coagulation effects of these four carbon dots prepared with Chinese medical materials as carbon sources were tested in vitro. Compared with blank groups (Figure 3a−d), these four carbon dots could greatly shorten the blood coagulation time ($P < 0.01$), which is correlated to the CD concentration. At high concentration, the ability of coagulation is equivalent to that of Yunnan Baiyao, the positive control group, and when the concentration decreases, the coagulation time is close to that of the blank control group (no obvious effect). The experiments showed that these four carbon dots all have hemostatic effects, which explains why the four carbonized traditional Chinese medicines could be used as hemostatic medicines. To further investigate the hemostatic effect of these carbon dots, SEM was used to observe the blood clots. SEM images (Figure 3e−i) show that the blood clots treated with carbon dots exhibited dense fibrin networks, which could hold large numbers of red blood cells, transforming the gathered blood cells into a highly coagulated state. Comparatively, the fibrin network can also be observed in the blank control group but not as dense as the administration group. The formation of the fibrin network is the key factor for the rapid hemostasis, beneficial to the formation of coagulation factors in blood and then the formation of a hemostatic plug to block the wound. The ultrastructural observation of the blood clots further verified the hemostatic ability of the prepared carbon dots.

To further study the hemostatic mechanism of these four carbon dots, PT and APTT were measured in vitro. The PT results (Figure 3k) show that carbon dots at different concentrations all could obviously shorten the PT values, that is, carbon dots could enhance the activity of related coagulation factors I, II, V, VII, and X in plasma through the exogenous coagulation pathway, to realize the hemostatic effect. Meanwhile, APTT (Figure 3j) values could also be shortened by carbon dots at different concentrations, showing that carbon dots could impact the coagulation factors VII, VIII, and IX through the endogenous coagulation pathway, transforming blood into a highly coagulated state. This is because of the negative charge on the surface of these four carbon dots due to the existence of OH and COOH groups, and when blood comes into contact with the negatively charged surface of foreign matters, the FXII factor would combine onto its surface and be activated as FXIIa, whose main function is to activate FXI into FXIa to start the endogenous coagulation pathway.[26]

In addition, FXIIa can promote the formation of FXIIa by activating prekallikrein, whose formation process is called surface activation. This surface activation process also requires the participation of high-molecular weight kininogen, which can accelerate the surface activation process as a cofactor. Furthermore, the hemostatic effects of these carbon dots were verified by the models of tail-cut bleeding and liver-cut bleeding in rats. In rats, the four carbon dots showed good hemostatic effects and obviously shortened the bleeding time (Figure 3l,m). Moreover, the carbon dots also exhibited certain anti-inflammatory activity (Figures S13−S16) and would help eliminate redness and swelling at the initial stage of trauma.

Therefore, the characterization experiment results showed that the four prepared carbon dots possess similar compositions, structures, and physical properties. Since three of the four carbon dots are made from plant materials, whose main components are hemicellulose, cellulose, and lignin, most of their surface functional groups are oxygen-containing groups. For the one made from human hair, whose components are protein and amino acids, the functional groups on its surface are nitrogen-containing groups. These results are verified from XPS and infrared spectra. These carbon dots also have similar particle sizes, lattice spacings, and surface charges, and most importantly, they have the same hemostatic effect and mechanism. However, the anti-inflammatory effect of the XYT-CDs prepared from human hair is stronger than that of other three CDs (Figures S13−S16), which is beneficial to its further applications. The research provides a new insight into the carbonization of traditional Chinese medicine for hemostasis. The source of their hemostasis ability is the formation of adsorptive carbon, which contains flavonoids and other active small-molecular compounds. The formation of CDs with similar structures and surface functional groups made from carbonization of different traditional Chinese medicine may be one of the reasons for using carbonized traditional Chinese medicine for hemostasis.

3. CONCLUSIONS

This paper reports the preparation of four blue-emitting carbon dots with four traditional Chinese medicines used for hemostasis by imitating the process of carbonization of traditional Chinese medicines, and the structures of the prepared carbon dots have been characterized. These four carbon dots exhibited excellent biocompatibility, and the in vitro experiments proved that they could realize hemostatic effects through impacting both endogenous and exogenous ways. Their hemostatic effect was verified in a rat tail-cut model and liver-cut model, and their anti-inflammatory abilities are also proven. Therefore, the carbon dots could work as potential hemostatic materials, which could be further used for developing novel medicines for hemostasis. This work provides new insights into the preparation of carbon dots from biomass carbon sources and new ideas for research on traditional Chinese medicine.

■ ASSOCIATED CONTENT

Supporting Information

The Supporting Information is available free of charge at https://pubs.acs.org/doi/10.1021/acsomega.2c06600.

Fluorescence spectra of PHT-CDs, OJT-CDs, DJT-CDs, and XYT-CDs; ultraviolet spectrogram of PHT-CDs, OJT-CDs, DJT-CDs, and XYT-CDs; ζ-potential of PHT-CDs, OJT-CDs, DJT-CDs, and XYT-CDs; and effect of different concentrations of CDs on NO secretion of cells (compared with control group, $^{**}P < 0.01$, $^{*}P < 0.05$) (PDF)

■ AUTHOR INFORMATION

Corresponding Author

Jun Li − *School of Pharmaceutical Sciences, South-Central Minzu University, Wuhan 430079, China; Ethnopharmacology Level 3 Laboratory, National Administration of Traditional Chinese Medicine, Wuhan 430079, China*; Email: lijun-pharm@hotmail.com

https://doi.org/10.1021/acsomega.2c06600
ACS Omega 2023, 8, 3176−3183

Authors

Bingchen Han − *School of Pharmaceutical Sciences, South-Central Minzu University, Wuhan 430079, China; Ethnopharmacology Level 3 Laboratory, National Administration of Traditional Chinese Medicine, Wuhan 430079, China;* orcid.org/0000-0002-8359-3053

Lidan Shen − *School of Pharmaceutical Sciences, South-Central Minzu University, Wuhan 430079, China*

Hanbing Xie − *School of Pharmaceutical Sciences, South-Central Minzu University, Wuhan 430079, China*

Qi Huang − *School of Pharmaceutical Sciences, South-Central Minzu University, Wuhan 430079, China*

Dan Zhao − *School of Pharmaceutical Sciences, South-Central Minzu University, Wuhan 430079, China;* orcid.org/0000-0002-9500-7410

Xianju Huang − *School of Pharmaceutical Sciences, South-Central Minzu University, Wuhan 430079, China; Ethnopharmacology Level 3 Laboratory, National Administration of Traditional Chinese Medicine, Wuhan 430079, China*

Xiao Chen − *Hubei Yaosheng Traditional Chinese Medicine Technology Co. Ltd, Zaoyang 441200, China*

Complete contact information is available at: https://pubs.acs.org/10.1021/acsomega.2c06600

Notes

The authors declare no competing financial interest.

■ ACKNOWLEDGMENTS

This research was funded by the Hubei science and technology planning project (2020BCB038) (2021BLB174), the Xiangyang research and development project (2021ABS003078), and the Fundamental Research Funds for the Central Universities "South-Central University for Nationalities" (No. CZP20003).

■ REFERENCES

(1) Zhu, S.; Song, Y.; Zhao, X.; Shao, J.; Zhang, J.; Yang, B. The photoluminescence mechanism in carbon dots (graphene quantum dots, carbon nanodots, and polymer dots): current state and future perspective. *Nano Res.* **2015**, *8*, 355−381.

(2) Han, B.; Hu, X.; Zhang, X.; Huang, X.; An, M.; Chen, X.; Zhao, D.; Li, J. The fluorescence mechanism of carbon dots based on the separation and identification of small molecular fluorophores. *RSC Adv.* **2022**, *12*, 11640−11648.

(3) Wang, W.; Cheng, L.; Liu, W. Biological applications of carbon dots. *Sci. China: Chem.* **2014**, *57*, 522−539.

(4) Li, H.; Huang, J.; Song, Y.; Zhang, M.; Wang, H.; Lu, F.; Huang, H.; Liu, Y.; Dai, X.; Gu, Z.; Yang, Z.; Zhou, R.; Kang, Z. Degradable Carbon Dots with Broad-Spectrum Antibacterial Activity. *ACS Appl. Mater. Interfaces* **2018**, *10*, 26936−26946.

(5) Varghese, M.; Balachandran, M. Antibacterial efficiency of carbon dots against Gram-positive and Gram-negative bacteria: A review. *J. Environ. Chem. Eng.* **2021**, *9*, No. 106821.

(6) Yang, X.; Li, P.; Tang, W.; Du, S.; Yu, M.; Lu, H.; Tan, H.; Xing, X. A facile injectable carbon dot/oxidative polysaccharide hydrogel with potent self-healing and high antibacterial activity. *Carbohydr. Polym.* **2021**, *251*, No. 117040.

(7) Smrithi, S. P.; Kottam, N.; Muktha, H.; Mahule, A. M.; Chamarti, K.; Vismaya, V.; Sharath, R. Carbon dots derived from Beta vulgaris: evaluation of its potential as antioxidant and anticancer agent. *Nanotechnology* **2021**, *33*, No. 045403.

(8) Zhao, X.; Qi, T.; Yang, M.; Zhang, W.; Kong, C.; Hao, M.; Wang, Y.; Zhang, H.; Yang, B.; Yang, J.; Jiang, J. Synthesis of dual functional procaine-derived carbon dots for bioimaging and anticancer therapy. *Nanomedicine* **2020**, *15*, 677−689.

(9) Li, D.; Lin, L.; Fan, Y.; Liu, L.; Shen, M.; Wu, R.; Du, L.; Shi, X. Ultrasound-enhanced fluorescence imaging and chemotherapy of multidrug-resistant tumors using multifunctional dendrimer/carbon dot nanohybrids. *Bioact. Mater.* **2021**, *6*, 729−739.

(10) Kang, M. S.; Singh, R. K.; Kim, T.-H.; Kim, J.-H.; Patel, K. D.; Kim, H.-W. Optical imaging and anticancer chemotherapy through carbon dot created hollow mesoporous silica nanoparticles. *Acta Biomater.* **2017**, *55*, 466−480.

(11) Bai, Y.; Zhang, B.; Chen, L.; Lin, Z.; Zhang, X.; Ge, D.; Shi, W.; Sun, Y. Facile One-Pot Synthesis of Polydopamine Carbon Dots for Photothermal Therapy. *Nanoscale Res. Lett.* **2018**, *13*, 287.

(12) Shi, W.; Han, Q.; Wu, J.; Ji, C.; Zhou, Y.; Li, S.; Gao, L.; Leblanc, R. M.; Peng, Z. Synthesis Mechanisms, Structural Models, and Photothermal Therapy Applications of Top-Down Carbon Dots from Carbon Powder, Graphite, Graphene, and Carbon Nanotubes. *Int. J. Mol. Sci.* **2022**, *23*, No. 1456.

(13) Zhao, S.; Yang, K.; Jiang, L.; Xiao, J.; Wang, B.; Zeng, L.; Song, X.; Lan, M. Polythiophene-Based Carbon Dots for Imaging-Guided Photodynamic Therapy. *ACS Appl. Nano Mater.* **2021**, *4*, 10528−10533.

(14) Zhang, M.; Cheng, J.; Hu, J.; Luo, J.; Zhang, Y.; Lu, F.; Kong, H.; Qu, H.; Zhao, Y. Green Phellodendri Chinensis Cortex-based carbon dots for ameliorating imiquimod-induced psoriasis-like inflammation in mice. *J. Nanobiotechnol.* **2021**, *19*, 105.

(15) Cheng, J.; Zhang, M.; Sun, Z.; Lu, F.; Xiong, W.; Luo, J.; Kong, H.; Wang, Q.; Qu, H.; Zhao, Y. Hemostatic and hepatoprotective bioactivity of Junci Medulla Carbonisata-derived Carbon Dots. *Nanomedicine* **2019**, *14*, 431−446.

(16) Lu, F.; Ma, Y.; Huang, H.; Zhang, Y.; Kong, H.; Zhao, Y.; Qu, H.; Wang, Q.; Liu, Y.; Kang, Z. Edible and highly biocompatible nanodots from natural plants for the treatment of stress gastric ulcers. *Nanoscale* **2021**, *13*, 6809−6818.

(17) Zhang, M.; Cheng, J.; Sun, Z.; Kong, H.; Zhang, Y.; Wang, S.; Wang, X.; Zhao, Y.; Qu, H. Protective Effects of Carbon Dots Derived from Phellodendri Chinensis Cortex Carbonisata against Deinagkistrodon acutus Venom-Induced Acute Kidney Injury. *Nanoscale Res. Lett.* **2019**, *14*, 377.

(18) Xu, Y.; Wang, B.; Zhang, M.; Zhang, J.; Li, Y.; Jia, P.; Zhang, H.; Duan, L.; Li, Y.; Li, Y.; Qu, X.; Wang, S.; Liu, D.; Zhou, W.; Zhao, H.; Zhang, H.; Chen, L.; An, X.; Lu, S.; Zhang, S. Carbon Dots as a Potential Therapeutic Agent for the Treatment of Cancer-Related Anemia. *Adv. Mater.* **2022**, *34*, No. 2200905.

(19) Tian, Y.; Zhou, S.; Takeda, R.; Okazaki, K.; Sekita, M.; Sakamoto, K. Anti-inflammatory activities of amber extract in lipopolysaccharide-induced RAW 264.7 macrophages. *Biomed. Pharmacother.* **2021**, *141*, No. 111854.

(20) Wang, X.; Guan, J.; Zhuang, X.; Li, Z.; Huang, S.; Yang, J.; Liu, C.; Li, F.; Tian, F.; Wu, J.; Shu, Z. Exploration of Blood Coagulation of N-Alkyl Chitosan Nanofiber Membrane in Vitro. *Biomacromolecules* **2018**, *19*, 731−739.

(21) Liu, C.; Yao, W.; Tian, M.; Wei, J.; Song, Q.; Qiao, W. Mussel-inspired degradable antibacterial polydopamine/silica nanoparticle for rapid hemostasis. *Biomaterials* **2018**, *179*, 83−95.

(22) Chen, J.; Ai, J.; Chen, S.; Xu, Z.; Lin, J.; Liu, H.; Chen, Q. Synergistic enhancement of hemostatic performance of mesoporous silica by hydrocaffeic acid and chitosan. *Int. J. Biol. Macromol.* **2019**, *139*, 1203−1211.

(23) Zheng, C.; Bai, Q.; Wu, W.; Han, K.; Zeng, Q.; Dong, K.; Zhang, Y.; Lu, T. Study on hemostatic effect and mechanism of starch-based nano-microporous particles. *Int. J. Biol. Macromol.* **2021**, *179*, 507−518.

(24) Li, X.; Lv, Y.; Pan, D. Pt catalysts supported on lignin-based carbon dots for methanol electro-oxidation. *Colloids Surf., A* **2019**, *569*, 110−118.

(25) Pan, J.; You, M.; Chi, C.; Dong, Z.; Wang, B.; Zhu, M.; Zhao, W.; Song, C.; Zheng, Y.; Li, C. The two dimension carbon quantum dots modified porous g-C3N4/TiO2 nano-heterojunctions for visible

light hydrogen production enhancement. *Int. J. Hydrogen Energy* **2018**, *43*, 6586−6593.
(26) Zheng, C.; Zeng, Q.; Pimpi, S.; Wu, W.; Han, K.; Dong, K.; Lu, T. Research status and development potential of composite hemostatic materials. *J. Mater. Chem. B* **2020**, *8*, 5395−5410.

https://doi.org/10.1021/acsomega.2c06600
ACS Omega 2023, 8, 3176−3183